Phenology and surface energy balance changes across northern lands TS1

Olivia Hau[1,2], Matthias Forkel[3], Wolfgang Buermann[2], Johanna Kranz[3], Mirco Migliavacca[4], Ulrich Weber[1], Annu Panwar[a], and Alexander J. Winkler[1]

[1]Max Planck Institute for Biogeochemistry, Jena, Germany
[2]Institute of Geography, Chair TS2 of Physical Geography and Climate Science, Augsburg University, Augsburg, Germany
[3]Faculty of Environmental Sciences, TUD Dresden University of Technology,
Professorship TS3 in Environmental Remote Sensing, Dresden, Germany
[4]European Commission, Joint Research Centre (JRC), Ispra, Italy
[a]formerly at: Max Planck Institute for Biogeochemistry, Jena, Germany TS4

Correspondence: Olivia Hau (ohau@bgc-jena.mpg.de) and Alexander J. Winkler (awinkler@bgc-jena.mpg.de)

Received: 16 February 2026 – Discussion started: 24 February 2026
Revised: 3 September 2026 – Accepted: 16 September 2026 – Published:

Abstract. TS5 TS6 Plant phenological shifts – notably earlier start (SOS) and later end (EOS) of the growing season – affect surface albedo, latent and sensible heat fluxes, and ultimately the surface temperature. The magnitude and spatial variability of these effects remain uncertain. Using Earth observation and reanalysis data (2001–2021), we quantify the sensitivity of surface energy fluxes to SOS and EOS changes across northern lands (> 30° N), and we report uncertainties and convergence across multiple independent datasets. Spatially-aggregated results show that an earlier SOS is generally associated with decreased albedo by up to ~~0.004~~ d^{-1} (needleleaf forests and tundra), and increased latent heat fluxes by ~~0.46~~ $W m^{-2} d^{-1}$ (spatial median), ranging from ~~0.17~~ $W m^{-2} d^{-1}$ (croplands) to 0.68 $W m^{-2} d^{-1}$ (mixed forests). Delays in EOS are also associated with decreases in albedo, though much smaller in magnitude, and with increases in latent heat flux – up to ~ ~~0.13~~ $W m^{-2} d^{-1}$ in mixed forests – with weaker and more variable responses across other land-cover types. Datasets reveal large spatial variability and discrepancies in the responses of the sensible heat fluxes and thus evaporative fraction. Across datasets, earlier SOS is consistently associated with increased latent heat flux, and the concurrent evidence from evaporative fraction suggests a shift towards enhanced latent cooling. These findings are consistent with a phenology-driven negative feedback on surface warming through enhanced evaporative cooling, although causal attribution from observational analyses alone is not possible.

1 Introduction

Across northern vegetated lands, significant shifts in the start date of the growing season (SOS) and end date of the growing season (EOS) have been observed during the last several decades (Piao et al., 2019). The overall more robust plant phenological trends towards earlier SOS have been linked to warming, although there is evidence that the temperature sensitivity of SOS has been declining more recently (Fu et al., 2015). The attribution of the overall weaker trends towards delayed EOS is less clear, and in addition to temperature other factors such as effects from photoperiod, nutrient and water availability also play an important role (Piao et al., 2019).

It is well established that plant phenology exerts a first-order control on water and energy exchanges between the land and atmosphere (Richardson et al., 2013). This is exemplified through in-situ studies documenting that in temperate deciduous forests the seasonal patterns of sensible and latent heat fluxes are largely driven by changes in leaf area index (Moore et al., 1996; Hogg et al., 2000). It is therefore conceivable that shifts in plant phenology have significant impacts on biophysical properties and the sur-

Proof only

Update fig1

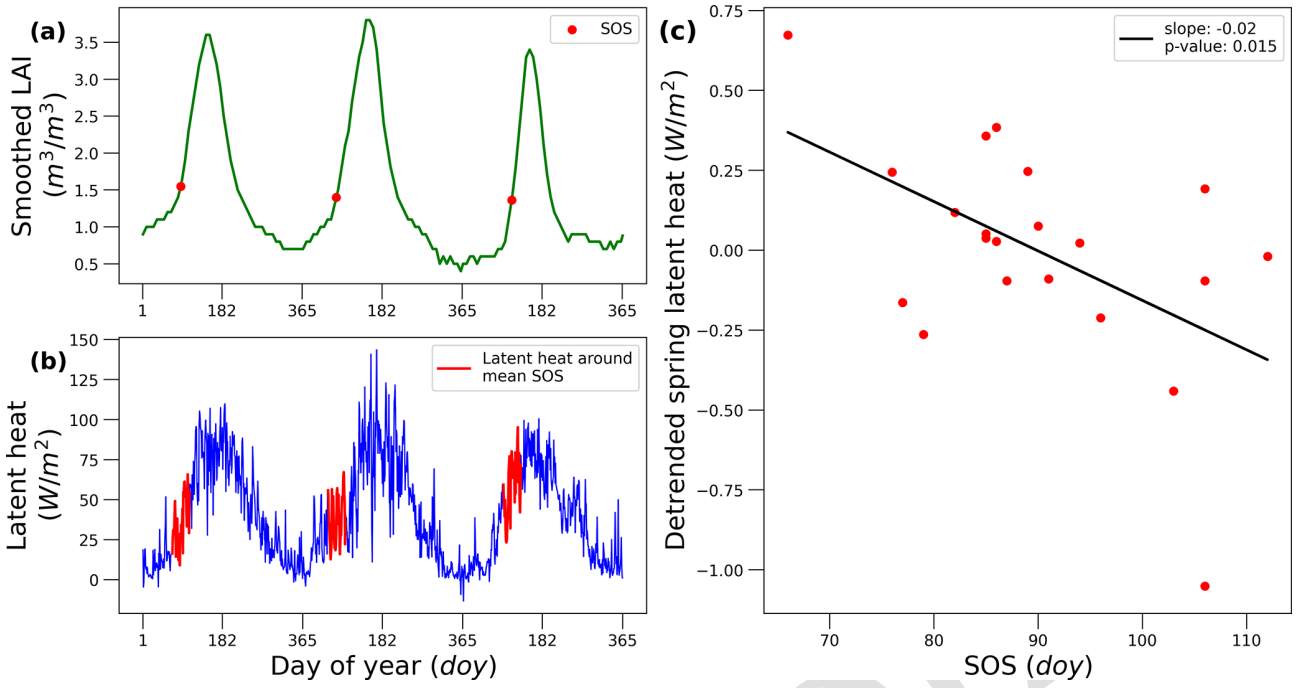


Figure 1. Example of the sensitivity calculation of latent heat to SOS between 2001 and 2003 at 52° N and 11° E. **(a)** SOS derived from smoothed MODIS-GLASS LAI data by using the EasyPhenology (Panwar, 2023) approach and threshold 0.3. **(b)** Selection of spring latent heat (±20 d around the mean SOS) calculated from ERA5 evaporation data. **(c)** The sensitivity and significance is derived from the linear regression between the detrended mean annual spring latent heat and the annual SOS date.

ERA5-based partial correlations due to potential residual within-product dependencies. However, the composite maps contain the average results across multiple data sources, including the FLUXCOM and GLEAM datasets, which provide additional independent support for the partial correlations of the turbulent fluxes.

3.1 Albedo

Spring albedo shows widespread significant positive sensitivities to SOS over boreal and Arctic regions. For example, sensitivities reach up to ~~0.0042~~ 0.004 (0.002 0.006) (unitless; median with 25 % and 75 percentiles) in deciduous needleleaf forests from the ERA5 albedo dataset, indicating that an earlier SOS is associated with declining albedo (Fig. 2a, b). Strong positive sensitivities also occur in evergreen needleleaf forests and tundra, as well as in high mountain regions such as the European Alps, Pyrenees, Caucasus, Altai, and Rocky Mountains. In contrast, mid-latitude regions in Europe, Central and Eastern Asia, and eastern North America exhibit negative sensitivities, implying increasing albedo with earlier SOS.

Positive sensitivities in tundra and boreal forests are likely driven by spring green-up masking residual snow cover, thereby reducing surface albedo. Conversely, negative sensitivities in croplands and deciduous broadleaf forests likely reflect canopy development shielding darker soils during spring green-up, particularly under moist soil conditions (Richardson et al., 2013). In agricultural systems, increased albedo may additionally arise from earlier sowing of brighter crops (Menzel et al., 2020).

Partial correlation analyses confirm these regional sensitivities of spring albedo to SOS, although areas of positive relationships are less spatially continuous and correlation magnitudes are more uniform across regions than the corresponding regression slopes (Fig. A2a).

Autumn albedo sensitivities to EOS are generally weaker and less spatially coherent than in spring. High-latitude regions, particularly tundra and evergreen needleleaf forests, tend to show negative sensitivities, indicating decreasing albedo with delayed EOS, likely due to prolonged canopy cover over bright soils or early snow. Deciduous broadleaf and mixed forests show on average positive sensitivities, consistent with extended leaf cover over relatively dark soils. Partial correlations reproduce these autumn patterns with similar spatial coverage and trend directions, although correlations at high latitudes are not markedly stronger than at lower latitudes (Fig. A2b).

As stated above, phenological shifts toward an earlier SOS result in the largest albedo responses in evergreen needleleaf forest, deciduous needleleaf forest, and tundra, with changes of 0.003–0.004 in albedo per day of SOS advance (Fig. 2b). To give a sense of magnitude in the context of the surface energy balance, we present a first-order estimate, based on the following assumptions: (i) the multi-decadal ERA5-Land

Proof

average downward shortwave radiation for May–June over northern lands (> 30° N) is used as the representative flux value; (ii) this downward flux is treated as approximately time-invariant over the study period; and (iii) the albedo change is assumed to act uniformly across the analysis domain. Using the ERA5-Land average of $257 \pm 18\,\mathrm{W\,m^{-2}}$ (the uncertainty is the spatially aggregated standard deviation of daily estimates for those months; May–June marks the SOS period, see Fig. A2a), the albedo change converts to a change in reflected shortwave energy. An albedo decrease of 0.003–0.004 per day thus corresponds to a reduction in reflected shortwave of about 0.77 ± 0.05 to $1.01 \pm 0.07\,\mathrm{W\,m^{-2}\,d^{-1}}$ for the regions considered. This additional shortwave absorption at the surface increases available energy potentially fueling turbulent heat fluxes, which we discuss next.

3.2 Latent heat fluxes

Spring latent heat fluxes exhibit widespread significant negative sensitivities to SOS (Fig. 3a–c), ranging from $-0.68^{-0.53}_{-0.86}\,\mathrm{W\,m^{-2}\,d^{-1}}$ in mixed forests to $-0.17^{-0.03}_{-0.37}\,\mathrm{W\,m^{-2}\,d^{-1}}$ in croplands (median with 25 % and 75 percentiles across four datasets). This indicates enhanced latent heat fluxes with earlier SOS. Sensitivities are negative across all vegetation types and strongest over forests. The four datasets show consistent large-scale patterns across most northern lands.

These results align with increased energy supply through shortwave radiation absorption (Sect. 3.1) and reported evidence that increasing vegetation cover during spring enhances transpiration (Schwartz, 1996; Panwar et al., 2020), primarily regulated by photosynthetic activity via stomatal conductance (Richardson et al., 2013). Partial correlations support this relationship, showing overall significant negative associations between spring *LE* and SOS, albeit with reduced spatial coverage compared to the sensitivity analysis (Fig. A3a, b).

Autumn latent heat generally exhibits positive sensitivities to EOS, reaching up to $0.15^{0.312}_{0.004}\,\mathrm{W\,m^{-2}\,d^{-1}}$ in mixed forests (Fig. 3d–f), indicating increasing *LE* with delayed EOS. Compared to SOS, EOS sensitivities are weaker, more spatially heterogeneous, and less consistent across datasets. In particular, GLEAM shows regionally negative sensitivities in forested areas. Partial correlations reveal strong associations in regions such as Central North America and eastern Europe and indicate comparable or slightly stronger *LE*–EOS correlations than *LE*–SOS correlations (Fig. A3c, d).

This variability likely reflects constraints imposed by soil moisture availability and seasonal meteorological conditions. While delayed EOS may enhance transpiration, limited water availability towards the end of the growing season can decouple phenology from evaporation (Migliavacca et al., 2012; Richardson et al., 2013). An additional and potentially active confounding factor is that an earlier SOS may progressively deplete soil moisture reserves through extended transpiration and canopy interception over summer, directly suppressing autumn latent heat flux independently of EOS timing. Where soil moisture is limiting at the start of autumn, reduced stomatal conductance and transpiration would dampen the expected positive EOS–*LE* response, or even reverse it. This is consistent with the weaker and more spatially heterogeneous EOS–*LE* sensitivities we report compared to SOS, and with the regionally negative EOS–*LE* sensitivities found in some datasets – particularly GLEAM, where explicit soil moisture constraints on evaporation are represented. The negative sensitivities that occur in some regions support the hypothesis of limited water reserves with an elongation of the growing season (Buermann et al., 2018), but the location and abundance varies between the different datasets.

3.3 Sensible heat fluxes

Sensitivities of sensible heat to SOS and EOS show no coherent large-scale pattern for northern lands and exhibit strong regional variability and dataset divergence (Fig. 4). However, smaller regions do exhibit coherent responses: spring *H* sensitivities to SOS are significantly negative across parts of northern Eurasia, particularly Siberia (Fig. 4a). Deciduous needleleaf forests show sensitivities of $-0.26^{0.03}_{-0.66}\,\mathrm{W\,m^{-2}\,d^{-1}}$, whereas other vegetation types display weaker and often mixed responses. Differences between datasets are especially pronounced in temperate and boreal Eurasia, with FLUXCOM generally indicating more negative or neutral sensitivities than ERA5 and GLEAM.

Partial correlations reveal little spatially extensive significant association between *H* and SOS, showing only weak tendencies towards negative correlations at some high latitude regions and positive correlations at some low latitude regions (Fig. A4a, b), reinforcing the absence of a robust spring signal.

Autumn sensible heat sensitivities to EOS are spatially mixed but show greater agreement between datasets than in spring (Fig. 4e, f). Central and south-eastern North America consistently exhibit negative sensitivities (e.g. $-0.08^{-0.02}_{-0.24}\,\mathrm{W\,m^{-2}\,d^{-1}}$ in croplands). Partial correlations coincide with these regions of significant sensitivities, again mainly showing negative relationships in mid- and lower-latitude regions (Fig. A4c, d).

Overall, these results show substantial uncertainty in how phenological shifts affect sensible heat. However, in high northern latitudes – particularly for deciduous and evergreen needleleaf forests and tundra (Fig. 4a, c) – a pattern of increased sensible heat flux with earlier SOS is emerging, mirroring the increase in latent heat flux (see Sect. 3.2). With both turbulent heat fluxes increasing, additional energy is required, consistent with the larger shortwave absorption from reduced albedo (Sect. 3.1). In the next section we examine how the partitioning of turbulent heat fluxes, expressed as the evaporative fraction (EF), responds to phenological shifts.

Proof only

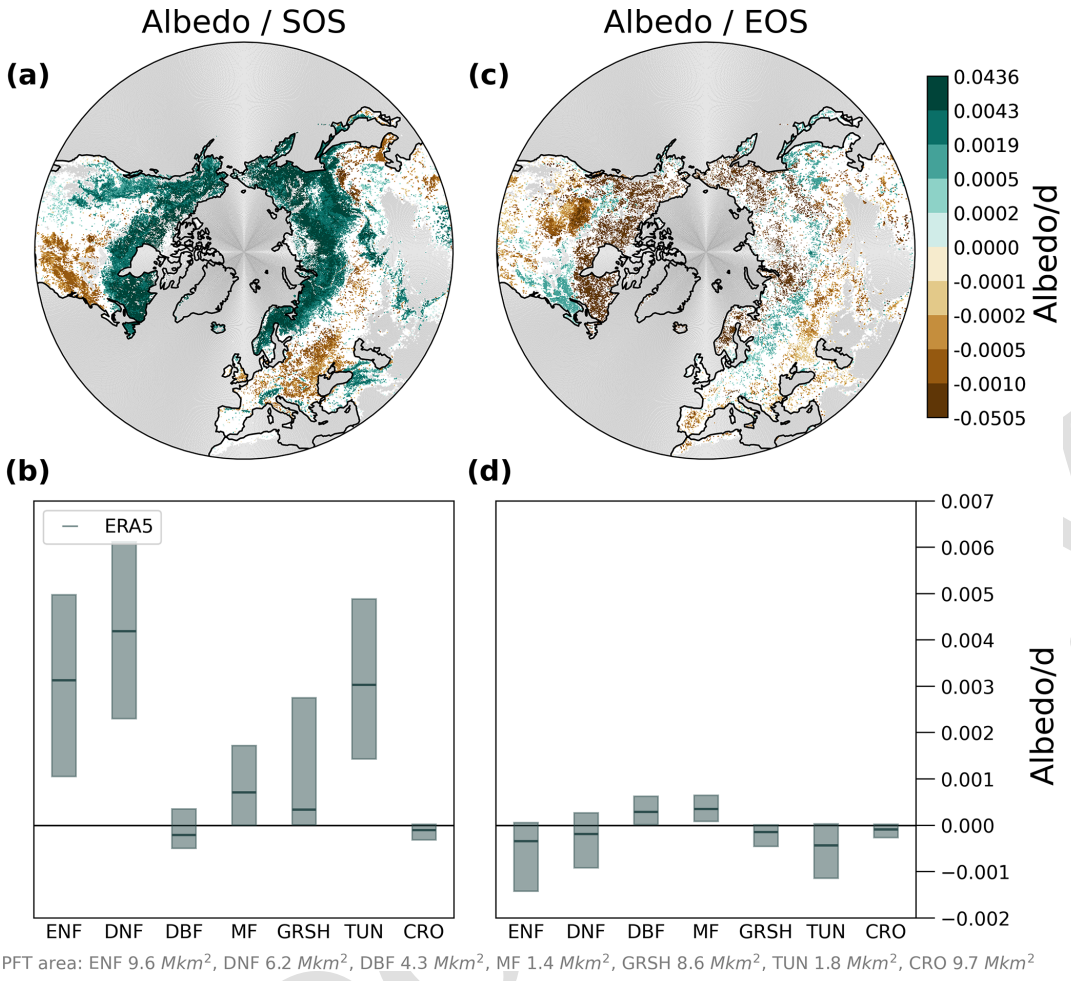


Figure 2. Sensitivity of spring and autumn albedo to SOS **(a–b)** and EOS **(c–d)**, respectively. Sensitivities are for the period 2001 to 2021. **(a, c)** Linear regression significant (p value ≤ 0.05) detrended slope of spring albedo with SOS **(a)** and autumn albedo with EOS **(c)** from the ERA5 dataset. Water, urban and built-up areas, permanent snow and ice, barren and sparsely vegetated areas, and areas with LAI < 0.5 are masked gray and non-significant slopes are masked white. **(b, d)** Statistical distributions of slopes for each land cover. Boxplots show the median (line), 25 % and 75 percentiles (box). ENF evergreen needleleaved forest, DNF deciduous needleleaved forest, DBF deciduous broadleaved forest, MF mixed forest, GRSH grass and shrubland, TUN tundra, CRO croplands.

3.4 Evaporative fraction and surface temperature

Generally, sensitivities of EF integrate concurrent changes in *LE* and *H* (Fig. 5). Spring EF largely mirrors *LE* patterns, showing widespread negative sensitivities to SOS, indicating increasing EF with earlier SOS (Fig. 5a). Sensitivities reach $-0.002^{-0.0008}_{-0.0049}$ in deciduous needleleaf forests (Fig. 5c). ERA5 and GLEAM exhibit substantially larger variability than FLUXCOM-derived estimates. Regional positive sensitivities occur in Central Asia and the western United States, but datasets show limited agreement in these areas. Partial correlations reproduce the dominant spatial patterns but with reduced coverage, particularly at high latitudes (Fig. A5).

Autumn EF generally increases with delayed EOS in temperate regions (Fig. 5b), reaching $0.0011^{0.0058}_{-0.0011}$ in croplands. Agreement among datasets is found across large parts of the Mediterranean, Central and Eastern Asia, and North America. In boreal and Arctic regions, however, EF sensitivities are spatially heterogeneous and datasets frequently disagree, particularly in boreal forests and tundra where ERA5 and GLEAM show much larger magnitudes than FLUXCOM. These discrepancies indicate substantial uncertainty in EF responses to phenological shifts. The potential confounding by SOS-driven soil moisture depletion (see Sect. 3.2) may likewise partially explain the dataset disagreement and spatial heterogeneity in autumn EF sensitivities: where soil moisture is limiting, suppressed transpiration reduces EF independently of EOS timing, masking or reversing the expected positive EOS–EF relationship.

Since rising surface temperature – primarily driven by increased downwelling longwave radiation from greenhouse gases over the long term – is the key driver of phenolog-

Update fig A6

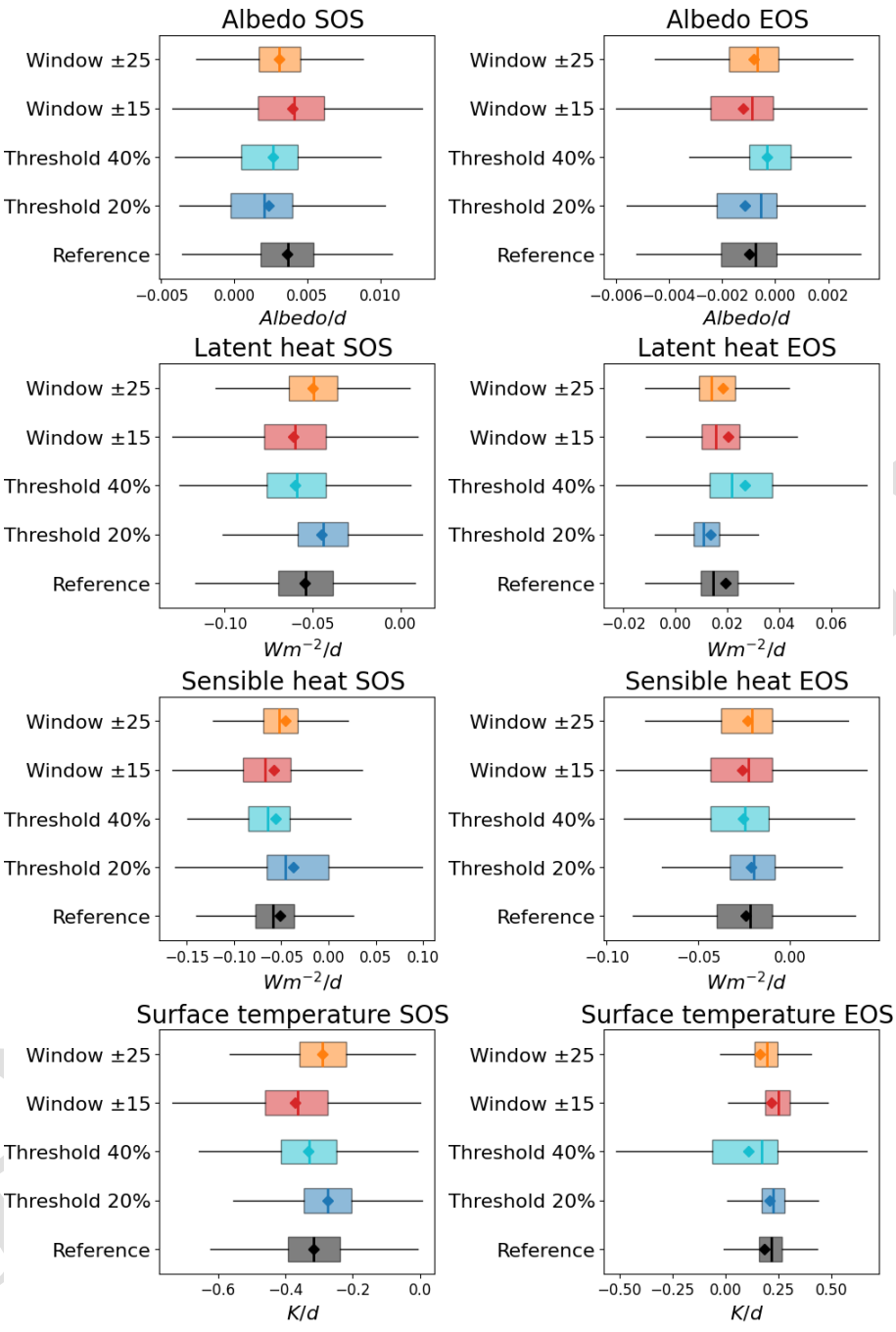


Figure A6. Statistical distribution of sensitivity slopes for the different analysis settings by surface energy balance variable. The reference analysis uses a 30 % threshold of the annual maximum LAI and a temporal window of ±20 d around the mean SOS/EOS. The alternative settings include a 20 % threshold, a 40 % threshold, a ±15 d window, and a ± 25 d window. In each sensitivity analysis, only one parameter (threshold or window width) is varied, while the other is kept identical to the reference analysis. Results are shown for the surface energy balance variables albedo, latent heat, sensible heat, and surface temperature. Box plots represent the distribution of significant sensitivity slopes (p value $p \leq 0.05$), with the box spanning the first and third quartiles (Q1–Q3), median (vertical line), mean (diamond), and whiskers (error bars).

A2 Supplementary Table

Table A1. Average sensitivities of surface energy balance variables (Albedo, *LE*, *H*, and surface temperature) to shifts in SOS and EOS across PFTs. The mean sensitivity (Mean) represents the average across all analysis settings (threshold 20 %, threshold 40 %, window width ±15 d, window width ±25 d, and the reference analysis). The spatially averaged sensitivities of the reference analysis (Mean ref) is based on a threshold of 30 % and window width of ±20 d, while the alternative analysis modify either threshold or window width. The average standard deviations across all analysis setting is reported as SD.

Update tableA1

Variable	PTD	PFT	Mean	SD	Mean ref
Albedo	SOS	ENF	0.003827	0.002075	0.004147
Albedo	SOS	DNF	0.004819	0.002374	0.005051
Albedo	SOS	DBF	0.000532	0.001892	0.000610
Albedo	SOS	MF	0.002029	0.001551	0.002284
Albedo	SOS	GRSH	0.002583	0.002180	0.003206
Albedo	SOS	TUN	0.004562	0.002232	0.004772
Albedo	SOS	CRO	−0.000326	0.000584	−0.000290
Albedo	EOS	ENF	−0.001870	0.001608	−0.001913
Albedo	EOS	DNF	−0.001065	0.001871	−0.001207
Albedo	EOS	DBF	0.000734	0.000672	0.000742
Albedo	EOS	MF	0.000645	0.000684	0.000728
Albedo	EOS	GRSH	−0.000601	0.000938	−0.000704
Albedo	EOS	TUN	−0.001599	0.001248	−0.001770
Albedo	EOS	CRO	−0.000427	0.000477	−0.000422
Latent heat	SOS	ENF	−0.049529	0.021353	−0.050380
Latent heat	SOS	DNF	−0.067392	0.022851	−0.068357
Latent heat	SOS	DBF	−0.063528	0.019337	−0.063547
Latent heat	SOS	MF	−0.065604	0.018285	−0.067485
Latent heat	SOS	GRSH	−0.046381	0.024068	−0.047007
Latent heat	SOS	TUN	−0.056940	0.020942	−0.057634
Latent heat	SOS	CRO	−0.034071	0.019761	−0.033724
Latent heat	EOS	ENF	0.014883	0.012576	0.012838
Latent heat	EOS	DNF	0.022033	0.017215	0.021149
Latent heat	EOS	DBF	0.035174	0.030471	0.036056
Latent heat	EOS	MF	0.041721	0.021512	0.043934
Latent heat	EOS	GRSH	0.016369	0.013892	0.016167
Latent heat	EOS	TUN	0.011079	0.005401	0.011231
Latent heat	EOS	CRO	0.024103	0.018542	0.024475
Sensible heat	SOS	ENF	−0.044999	0.042384	−0.047462
Sensible heat	SOS	DNF	−0.071982	0.027683	−0.072033
Sensible heat	SOS	DBF	−0.010660	0.067768	−0.012965
Sensible heat	SOS	MF	0.000341	0.062704	−0.000439
Sensible heat	SOS	GRSH	−0.045400	0.040353	−0.046594
Sensible heat	SOS	TUN	−0.058554	0.027638	−0.061409
Sensible heat	SOS	CRO	0.009088	0.046347	0.010008
Sensible heat	EOS	ENF	−0.019299	0.033075	−0.019417
Sensible heat	EOS	DNF	0.008444	0.048636	0.009988
Sensible heat	EOS	DBF	−0.036497	0.038674	−0.035140
Sensible heat	EOS	MF	0.002688	0.049018	−0.000625
Sensible heat	EOS	GRSH	−0.021628	0.020887	−0.020890
Sensible heat	EOS	TUN	−0.002501	0.015915	−0.004624
Sensible heat	EOS	CRO	−0.033220	0.021971	−0.033497
Surface temperature	SOS	ENF	−0.293529	0.100413	−0.296032
Surface temperature	SOS	DNF	−0.383277	0.100361	−0.384563
Surface temperature	SOS	DBF	−0.280139	0.081732	−0.280150
Surface temperature	SOS	MF	−0.317295	0.073297	−0.324208
Surface temperature	SOS	GRSH	−0.288645	0.124567	−0.289526
Surface temperature	SOS	TUN	−0.334203	0.124194	−0.333499
Surface temperature	SOS	CRO	−0.190243	0.083877	−0.191818
Surface temperature	EOS	ENF	0.177758	0.128976	0.181428
Surface temperature	EOS	DNF	0.255838	0.111221	0.254483
Surface temperature	EOS	DBF	0.106318	0.182727	0.134429
Surface temperature	EOS	MF	0.107489	0.209369	0.133673
Surface temperature	EOS	GRSH	0.158064	0.142853	0.171824
Surface temperature	EOS	TUN	0.221234	0.070997	0.225692
Surface temperature	EOS	CRO	−0.069645	0.099492	−0.067721

Proofonly

Please replace figures 7 and A6, as well as table A1, with the attached versions. There was a unit conversion issue in the previous figures.
Also, please replace Fig. 1 as I updated it for unit consistency.
Please adapt the updated values and references throughout the text as well, along with the changes to figure captions 2-6.
I apologize for the numerous changes in this final editing step. If you have any questions about the changes, please let me know.
Thank you very much!